Inorganic Chemistry

ARTICLE

pubs.acs.org/IC

New Hybrid Zirconium Aminophosphonates Containing Piperidine and Bipiperidine Groups

Marco Taddei,* Ferdinando Costantino, Valentina Manuali, and Riccardo Vivani

Dipartimento di Chimica, CEMIN, Via Elce di sotto n. 8, 06123 Perugia, Italy

Supporting Information

ABSTRACT: The reaction of *N*-(phosphonomethyl)piperidine and *N*,*N*′-bis(phosphonomethyl)bipiperidine with zirconium(IV) in hydrofluoric acid media led to the preparation of two new zirconium fluoride phosphonate derivatives with 1D and 2D structure, respectively. Their structures were solved ab initio from laboratory powder X-ray diffraction (PXRD) data. The monophosphonate derivative, with formula $ZrF_2(HF)(O_3PCH_2NC_5H_{10})$, has a 1D structure (triclinic, space group $P\bar{1}$, a = 6.6484(3) Å, b = 7.1396(3) Å, c = 12.2320(6) Å, α = 77.932(4)°, β = 87.031(6)°, γ = 78.953(5)°, V = 557.22(4) Å^3, and Z = 2) made of inorganic chains constituted from the connection of zirconium octahedra and phosphorus tetrahedra with the piperidine groups bonded on their external part. The diphosphonate derivative, with formula $Zr_2F_4(HF)_2(O_3PCH_2)NC_{10}H_{18}N(CH_2PO_3)$, has a 2D structure (triclinic, space group $P\bar{1}$, a = 6.6243(3) Å, b = 7.2472(4) Å, c = 12.2550(7) Å, α = 102.879(4)°, β = 100.29(1)°, γ = 101.287(7)°, V = 547.03(4) Å^3, and Z = 1) composed of the packing of covalent layers whose structure may be ideally obtained by the joining of adjacent chains of the 1D compound. In these hybrid layers, inorganic regions made of the connectivity of zirconium octahedra and phosphorus tetrahedra alternate with organic regions represented by the bipiperidine moieties. A section dedicated to vibrational spectroscopy analysis is also included, mainly devoted to clarify some issues not easily deducible on the basis of PXRD data and to describe the fluorine environment inside zirconium phosphonate structures.

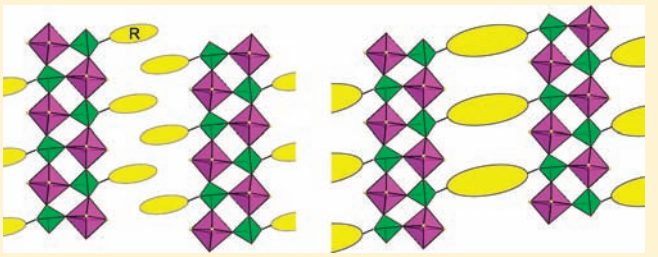

INTRODUCTION

The search of new compounds for practical application often takes advantage of the possibility of modulating the composition of archetype compounds, with known structure, in order to improve their performances. The class of zirconium phosphonates is an example of insoluble compounds whose structure can be easily modulated and adapted to be used in different fields of materials chemistry, such as catalysis, ion and proton conductivity, use as sensors, and so on.[1] Recently, we have focused on a subset of zirconium phosphonates prepared using aminomethylenephosphonate building blocks. These compounds show a large variety of structural features, probably because of the presence of strong noncovalent interactions within the constituting building blocks, that act as structure-directing factors.[2] In this class of compounds, correlation of the molecular structure of the phosphonate building blocks with the final structure of zirconium phosphonate is not an easy task. The present study is an example of how different the rationally expected results can be from those really found.

We recently observed that *N*,*N*′-bis(phosphonomethyl)piperazine can form two different zirconium derivatives.[3] One of them has an intriguing 3D framework structure, featuring infinite channels accessible to solvent molecules. These channels originated by spacing, through piperazine groups, of inorganic zirconium phosphonate chains. However, a permanent porosity was not detected in this structure, probably because of the small dimensions of the channels. A logical follow-up study should be the finding of isoreticular compounds with an expanded framework, using larger spacers, as depicted in Figure 1. Many examples of this approach are recently reported in the field of coordination polymers, also involving similar divalent metal aminophosphonates.[4]

Under this rational design, we planned the synthesis of zirconium phosphonates containing an organic group larger than piperazine, such as bipiperidine. Unfortunately, the stereochemistry of zirconium phosphonates is hardly predictable, and the initial goal was not reached because in all of our attempts we obtained only one crystalline phase, whose composition and structure is markedly different from the archetype compound.

However, the structure of this phase and that of its homologous piperidine monophosphonate derivative, which was included in this investigation, will be discussed and compared, with the aim of giving a contribution to composition of the intricate mosaic of the stereochemistry of zirconium phosphonates, as a support for the true rational design of tailor-made materials.

In addition, thorough Fourier transform infrared (FT-IR) and Raman studies of these compounds provided useful information on fine structural details.

Received: June 28, 2011
Published: October 04, 2011

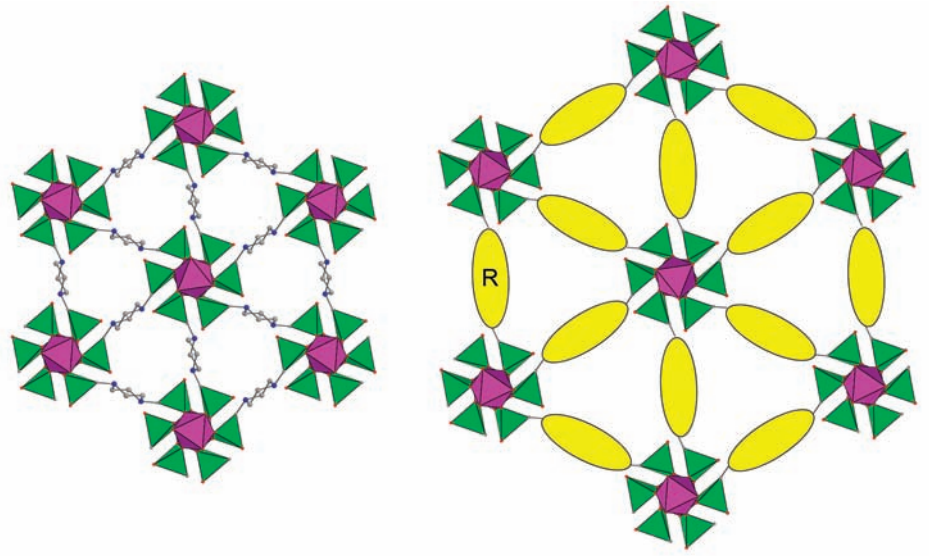

Figure 1. Possible expansion of the 3D framework of zirconium piperazine-*N*,*N*′-bismethylenephosphonate by means of isoreticular synthesis.

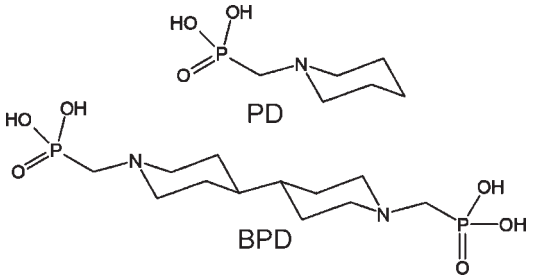

Figure 2. Structural formulas of PD and BPD.

EXPERIMENTAL SECTION

Chemicals. $ZrOCl_2 \cdot 8H_2O$ was a Merck Pro Analysi product. All of the other chemicals were Carlo Erba RPE grade. All reagents were used as received without further purification.

Synthesis of the Phosphonic Acids. N-(Phosphonomethyl)piperidine, $H_2O_3PCH_2NC_5H_{10}$ (hereafter PD), and *N*,*N*′-bis(phosphonomethyl)-bipiperidine, $H_2O_3PCH_2NC_{10}H_{18}NCH_2PO_3H_2$ (hereafter BPD), were prepared according to the Moedritzer−Irani method[5] and purified by reprecipitation in tetrahydrofuran (yields: PD 70%; BPD 86%). The solids were then characterized by determination of their melting points, C, H, and N elemental analysis, and powder X-ray diffraction (PXRD) qualitative phase analysis. The molecular structure was checked with ^1H and ^{31}P liquid NMR. The structural formulas of PD and BPD are shown in Figure 2.

Synthesis of the Zirconium Derivatives. The zirconium salt of PD, with formula $ZrF_2(HF)(O_3PCH_2NC_5H_{10})$ (hereafter ZPD), was prepared as follows: a clear solution (75 mL of *n*-propanol + 5 mL of H_2O) of PD (2.24 g, 12.5 mmol) was added to a solution of $ZrOCl_2 \cdot 8H_2O$ (1.61 g, 5 mmol) and HF (2.9 M, 14 mL, 40 mmol). The molar ratio in the final mixture was Zr:PD:F = 1:2.5:8. For the zirconium salt of BPD, with formula $Zr_2F_4(HF)_2(O_3PCH_2)NC_{10}H_{18}N(CH_2PO_3) \cdot 1.6H_2O$ (hereafter ZBPD), a mixture (15 mL of *n*-propanol + 60 mL of H_2O) of BPD (1.78 g, 5 mmol) was added to a solution of $ZrOCl_2 \cdot 8H_2O$ (0.644 g, 2 mmol) and HF (2.9 M, 5.2 mL, 15 mmol). The molar ratio in the final mixture was Zr:BPD:F = 1:2.5:7.5. These solutions were maintained in closed plastic vessels at 80 °C for 3 days. The white precipitates were separated by centrifugation and washed with the propanol/H_2O mixture. Finally, they were dried in an oven at 70 °C. Yields: 0.500 g, 85% (calculated on Zr) for ZPD and 0.880 g, 54% (calculated on Zr) for ZBPDa.

The anhydrous form of compound ZBPD, obtained by heating at 100 °C, will be hereafter identified as ZBPDa.

Found for ZPD: Zr, 27.62; P, 9.81; F, 17.3; C, 22.0; N, 4.1; H, 4.3. $ZrPF_3O_3NC_6H_{13}$ requires the following: Zr, 27.96; P, 9.50; F, 17.47; N, 4.29; C, 22.07; H, 3.99. Found for ZBPD: Zr, 27.87; P, 9.72; F, 17.3; N, 4.5; C, 22.02; H, 3.99. $Zr_2P_2F_6O_{7.6}N_2C_{12}H_{27.2}$ requires the following: Zr, 26.81; P, 9.13; F, 16.79; N, 4.12; C, 21.21; H, 4.08.

Analytical Procedures. The zirconium and phosphorus contents of samples were obtained by inductively coupled plasma optical emission spectroscopy using a Varian Liberty Series II instrument working in axial geometry, after mineralization of the samples with hydrofluoric acid. The fluorine content was determined as fluoride by ion chromatography: about 0.1 g of sample was refluxed for 3 h with 10 mL of 1 M NaOH up to complete hydrolysis. The resulting solution was filtered, properly diluted, and analyzed with a Dionex series 2000 i/sp instrument, using an IonPack AS4A column and a buffer solution, of the following composition: 1.7×10^{-3} M in $NaHCO_3$ and 3.5×10^{-3} M in Na_2CO_3 as eluent. The carbon, nitrogen, and hydrogen contents were determined by elemental analysis using an EA 1108 CHN Fisons instrument. PXRD patterns for structure determinations and Rietveld refinements were collected with a PANalytical X'PERT APD diffractometer and a PW3020 goniometer equipped with a curved graphite monochromator on the diffracted beam, using Cu Kα radiation. Data were collected according to the step scanning procedure, with a scan step of 0.02° and a counting time of 20 s step^{-1}. Divergence and scatter slits of 0.5° and a 0.1 mm receiving slit were used. The LFF tube operated at 40 kV and 40 mA. To minimize preferred orientations, the samples were carefully side-loaded onto an aluminum sample holder with a quartz monocrystal oriented underneath. Thermogravimetric analyses (TGA) were performed using a Netzsch STA490C thermoanalyzer under a 20 mL min^{-1} air flux with a heating rate of 5 °C min^{-1}. Micro-Raman spectra were obtained using a JASCO Ventuno double-grating spectrophotometer equipped with a charge-coupled device detector cooled at −50 °C. Raman spectra were excited using green radiation from an Nd:YAG laser. Backscattering illumination and collection of the scattered light were made through an Olympus confocal microscope (long-focus Olympus 50× and 100× objectives). When a 1200 lines mm^{-1} grating

Table 1. Crystal Data and Refinement Details for ZPD and ZBPDa

	ZPD	ZBPDa
empirical formula	$ZrPF_3O_3NC_6H_{13}$	$ZrPF_3O_3NC_6H_{12}$
fw	325.26	324.26
cryst syst	triclinic	triclinic
space group	$P\bar{1}$	$P\bar{1}$
a/Å	6.6484(3)	6.6245(3)
b/Å	7.1396(3)	7.2474(4)
c/Å	12.2320(6)	12.2548(7)
α/deg	77.932(4)	102.876(4)
β/deg	87.031(6)	100.29(1)
γ/deg	78.953(5)	101.293(7)
V/Å^3	557.22(4)	547.04(4)
Z	2	2
calcd density/g cm^{-3}	1.94	1.97
wavelength/Å	1.540 56	1.540 56
pattern range, 2θ/deg	5−80	6−140
step scan increment, 2θ/deg	0.02	0.02
time per step/s	60	60
no. of data points	3501	8053
no. of reflections	1153	4120
no. of parameters	71	68
no. of restraints	45	45
R_p	0.0968	0.0370
R_{wp}	0.1277	0.0530
R_F^2	0.057 45	0.089 33
GOF	6.72	2.61

was used, a spectral resolution of about 2 cm^{-1} was achieved. Spectral measurements were made with continuous scans in the range 50−3500 cm^{-1}, exposure times in the range 10−200 s, and 5−10 accumulations; the laser power at the sample was 5mW at maximum. Calibration of the spectrometer was accomplished using the Raman lines of a polystyrene standard. Transmittance mid-FT-IR measurements were carried out with a JASCO FT/IR 4000 spectrophotometer composed of a high-intensity ceramic source, a Michelson interferometer, and a deuterated L-alanine tryglycine sulfate detector. The spectral range collected was 400−4000 cm^{-1}, with a spectral resolution of 2 cm^{-1} acquiring 100 scans. The samples were dispersed on anhydrous KBr pellets.

H/D exchange on compound ZBPD was performed by contacting the powder with D_2O for 3 days. The material was then filtered and dried. All of these steps were carried out under nitrogen.

Spectra at higher temperatures, in the range 30−110 °C, were obtained working in a vacuum environment with a variable-temperature cell P/N 21525 equipped with KBr windows and supplied with a high-stability controller.

Structure Determination and Refinement for ZPD and ZBPDa. The crystal structures of ZPD and ZBPDa were solved ab initio from PXRD data. The diffraction patterns were fitted using a Pearson VII profile function, and the positions of the first 20 lines were used for the indexing procedure, which was achieved with both *TREOR*[6] and *DICVOL06*[7] programs. The compounds crystallize in the triclinic space, in which systematic extinctions are not expected. Structural models of ZPD and ZBPDa were determined using the real-space global optimization methods implemented in the *FOX* program.[8] The software optimized a structural model described by the use of building blocks defined in terms of their internal coordinates, such as bond lengths, bond angles, and dihedral angles. Optimization was performed by comparing the PXRD patterns calculated from randomly generated configurations and using the "integrated R_{wp}" (iR_{wp}) as the cost function. Trial structures were generated using the "Parallel Tempering" algorithm.[9] The starting model was composed of the free metal atom and the organophosphonic acid group. Hydrogen atoms were omitted. Starting values for the bond lengths and angles were taken from similar systems found in the literature and constrained within a standard deviation of 0.15 Å and 10°, respectively. Torsion angles were not constrained. Antibump restraints between the metal and phosphorus atoms were applied in order to speed up the optimization process. Rietveld refinements of the structural models were performed using the *GSAS* program.[10] First, zero-shift, cell, background, and profile-shape parameters were refined. A corrected pseudo-Voigt profile function (six terms) with two terms for the correction of asymmetry at the low-angle region was used. Then, atomic coordinates were refined by restraining the bond distances to the following values: Zr−O = 2.05(5) Å, Zr−F = 1.95(5) Å, P−O = 1.56(5) Å, C−C = 1.54(5) Å, and C−N = 1.45(5) Å. The statistical weight of these restraints was decreased as the refinement proceeded, but it was not possible to set it to zero because of some unrealistic light-atom bond distances. Refinement of the atomic displacement parameters of zirconium atoms was performed, leaving them to change freely, while for all other atoms, they were not refined and set to 0.025 Å^2. At the end of refinement, the shifts in all parameters were less than their standard deviations.

Table 2. Selected Bond Lengths (Å) and Angles (deg) for ZPD

Zr(1)−F(1)	1.85(1)	P(1)−O(1)	1.55(1)
Zr(1)−F(2)	2.07(1)	P(1)−O(2)	1.59(1)
Zr(1)−F(3)	1.91(1)	P(1)−O(3)	1.53(1)
Zr(1)−O(1)	2.07(1)	P(1)−C(4)	1.91(1)
Zr(1)−O(2)	2.23(1)		
Zr(1)−O(3)	2.08(1)	F(2)···N(5)	3.00(2)
F(1)−Zr(1)−F(2)	84.9(7)	O(1)−Zr(1)−F(3)	86.0(6)
F(1)−Zr(1)−O(1)	93.6(7)	O(2)−Zr(1)−O(3)	91.7(6)
F(1)−Zr(1)−O(2)	91.8(6)	O(2)−Zr(1)−F(3)	90.2(6)
F(1)−Zr(1)−O(3)	88.2(6)	O(3)−Zr(1)−F(3)	92.1(7)
F(1)−Zr(1)−F(3)	178.0(8)	O(1)−P(1)−O(2)	107(1)
F(2)−Zr(1)−O(1)	91.1(6)	O(1)−P(1)−O(3)	109(1)
F(2)−Zr(1)−O(2)	174.8(7)	O(1)−P(1)−C(4)	110(1)
F(2)−Zr(1)−O(3)	84.2(6)	O(3)−P(1)−C(4)	112.6(8)
F(2)−Zr(1)−F(3)	93.1(7)	O(2)−P(1)−C(4)	109.3(9)
O(1)−Zr(1)−O(2)	93.1(6)	O(2)−P(1)−O(3)	109(1)
O(1)−Zr(1)−O(3)	174.8(7)		

Table 1 lists the crystal data and refinement details, and Tables 2 and 3 list selected bond distances and angles for ZPD and ZBPDa. Figure 3 shows the final Rietveld and difference plots.

Structural data for the zirconium derivative of BPD are referred to the anhydrous form ZBPDa because in the hydrate form ZBPD we were not able to locate the water molecules, very likely because they were disordered.

RESULTS AND DISCUSSION

Structure description of ZPD. Figure 4 shows the structure of ZPD. The structure is composed of the packing of hybrid inorgano−organic 1D macrounits made of the connectivity of zirconium octahedra and phosphorus tetrahedra. Each polymeric chain is built by propagation, along the c axis, of "composite building units" (CBUs) formed by two zirconium octahedra and

dx.doi.org/10.1021/ic201381t |*Inorg. Chem.* 2011, 50, 10835–10843

Table 3. Selected Bond Lengths (Å) and Angles (deg) for ZBPDa

Zr(1)−O(1)	2.102(6)	P(1)−O(1)	1.635(7)
Zr(1)−O(2)	2.051(5)	P(1)−O(2)	1.563(7)
Zr(1)−O(3)	2.053(5)	P(1)−O(3)	1.561(6)
Zr(1)−F(1)	2.083(5)	P(1)−C(4)	1.855(8)
Zr(1)−F(2)	1.942(5)		
Zr(1)−F(3)	1.944(5)	F(1)···N(5)	3.01(2)
O(1)−Zr(1)−O(2)	89.5 (5)	O(3)−Zr(1)−F(3)	89.8(3)
O(1)−Zr(1)−O(3)	92.6 (4)	F(1)−Zr(1)−F(2)	90.6(3)
O(1)−Zr(1)−F(1)	177.2(5)	F(1)−Zr(1)−F(3)	89.6(3)
O(1)−Zr(1)−F(2)	90.6(3)	F(2)−Zr(1)−F(3)	179.4(5)
O(1)−Zr(1)−F(3)	89.2(3)	O(1)−P(1)−O(2)	110.1(5)
O(2)−Zr(1)−O(3)	177.6(4)	O(1)−P(1)−O(3)	111.7(5)
O(2)−Zr(1)−F(1)	88.0(3)	O(1)−P(1)−C(4)	111.1(4)
O(2)−Zr(1)−F(2)	91.5(3)	O(2)−P(1)−O(3)	108.4(4)
O(2)−Zr(1)−F(3)	89.0(3)	O(2)−P(1)−C(4)	108.7(5)
O(3)−Zr(1)−F(1)	89.9(3)	O(3)−P(1)−C(4)	106.8(4)
O(3)−Zr(1)−F(2)	89.7(3)		

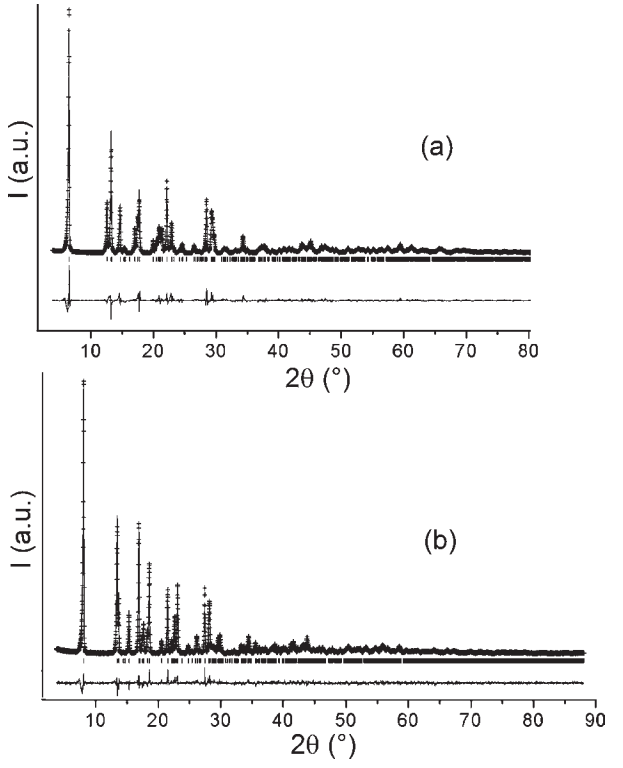

Figure 3. Final Rietveld and difference plots for ZPD (a) and ZBPDa (b).

two phosphorus tetrahedra, which alternate in a four-membered ring fashion. Each CBU contains two formula units and corresponds to the unit cell content. Each phosphonate tetrahedron shares three corners with three different Zr octahedra, so that each zirconium octahedron is bonded to three oxygen atoms belonging to three different phosphonates. In addition, three fluorine atoms are coordinated to zirconium. Piperidine groups are bonded, via the nitrogen atom, to phosphonate tetrahedra and are directed roughly perpendicular to the chain axis.

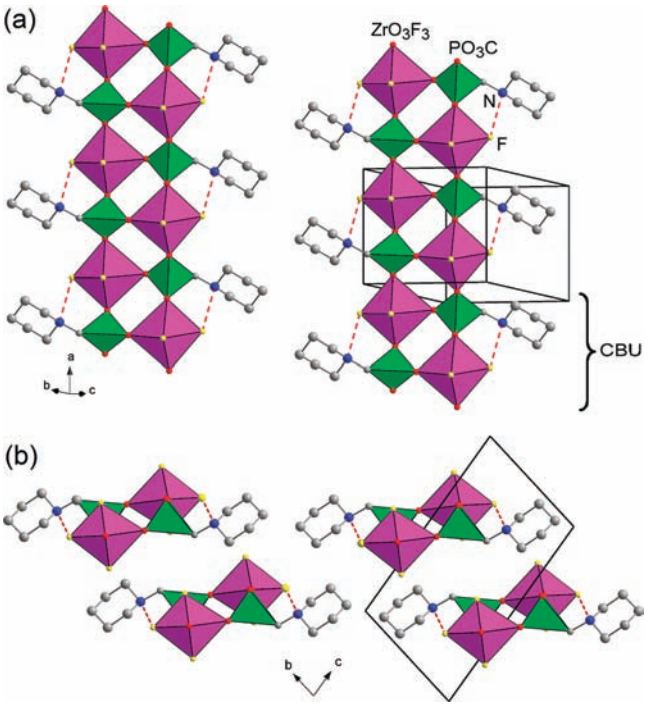

Figure 4. Polyhedral representation of the structure of ZPD perpendicularly (a) and along the *a* axis (b). Hydrogen atoms are omitted. Hydrogen bonds are represented as dashed lines.

Piperidine rings have a slightly twisted chair conformation. The nitrogen atom of the piperidine ring is 3.00(2) Å apart from the F(2) atom belonging to an adjacent zirconium octahedron, indicating a possible weak hydrogen bond between the two atoms. PXRD data do not provide any information about the position of the hydrogen atom involved in this interaction, which may be assumed to be shared between the nitrogen and fluorine atoms. However, FT-IR data, which will be discussed later on, suggest that F(2) is protonated. According to this, the Zr−F(2) bond length is longer [2.07(1) Å] than Zr−F(1) and Zr−F(3) bond lengths, whose average length is 1.88(1) Å. The polymeric chains are closely packed and no void spaces are present between them, justifying the absence of intercalated guest species. Adjacent chains approximately lie on the [120] crystallographic planes and are shifted by $^1/_2c$, while adjacent planes are about 5 Å apart. No strong noncovalent bonds are present between adjacent chains.

Structure Description of ZBPDa. Figure 5 shows the structure of ZBPDa viewed down the *a* and *b* axes. It has a layered structure that closely resembles that of ZPD, although with a higher dimensionality. This structure originates by the packing, along the *a* axis, of covalent inorganic−organic layers. Each layer is composed of inorganic chains built by connected zirconium octahedra and phosphorus tetrahedra, running parallel to the [100] crystallographic plane, that are covalently joined, on the same plane, by bipiperidine groups. The connectivity of zirconium octahedra and phosphorus tetrahedra is the same as that described in ZPD, and also the relative positions of the bipiperidine rings with respect to the chain are close to those found in ZPD. Therefore, each layer can be ideally considered as originating by the connection, through C−C bonds, of adjacent ZPD chains. In this context, a CBU similar to that described for ZPD, constituted of two zirconium octahedra, two phosphorus

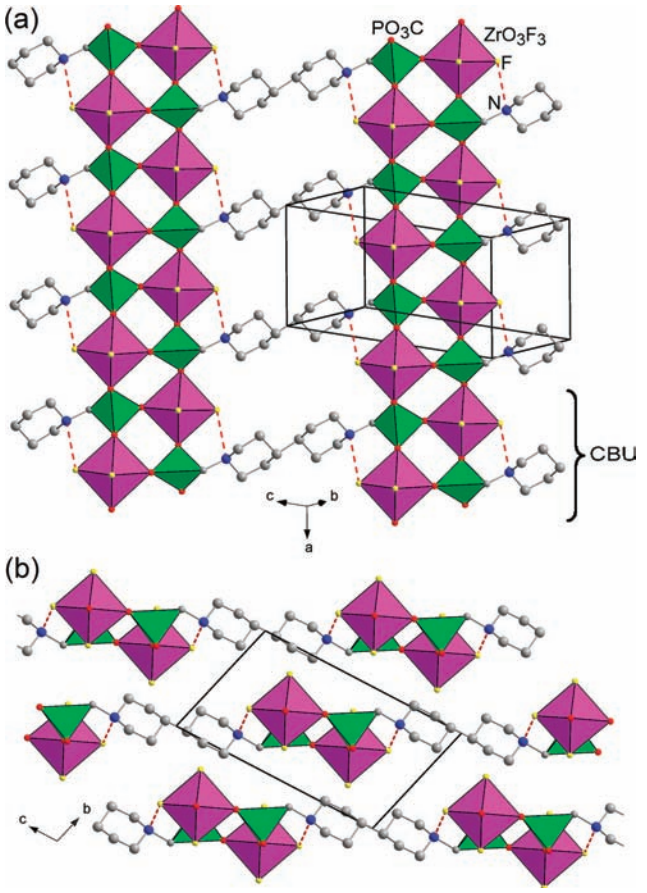

Figure 5. Polyhedral representation of the structure of ZBPDa perpendicular (a) and parallel (b) to the layers. Hydrogen atoms are omitted. Hydrogen bonds are represented as dashed lines.

tetrahedra, and a bipiperidine residue, can be identified as the smallest building unit for the whole layer. Also in this structure, the N(5)···F(1) distance is 3.01(2) Å, indicating that a hydrogen bond is present between the two atoms, and FT-IR data suggest that the hydrogen atom may be assigned to the fluorine. According to this, the Zr−F(1) bond length is longer [2.083(5) Å] than Zr−F(2) and Zr−F(3), whose average length is 1.943(5) Å. No strong noncovalent interactions are present between adjacent layers, so they are packed only by van der Waals forces.

Thermal Behavior. TGA curves for ZPD and ZBPD are shown in Figure 6. The thermal behaviors of the two compounds are similar. The main difference is that ZBPD shows a first weight loss (4.14%) at about 60 °C, corresponding to 1.6 water molecules per formula unit. The nonstoichiometry of the water content and the low dehydration temperature, indicating that water molecules are loosely held between the layers, can support the idea, formulated during structural analysis, that water is disordered inside the structure. At 100 °C, the ZBPDa phase is present. Water loss is fully reversible, and if ZBPDa is left standing in moist air, rehydration occurs with the restoration of ZBPD.

Beyond 300 °C, both ZPD and ZBPDa start to lose weight due to oxidation of organics. We can assume that at the end of the analysis (1200 °C) an equimolar mixture of ZrO_2 and ZrP_2O_7 is formed because the P/Zr molar ratio is 1 in both compounds.

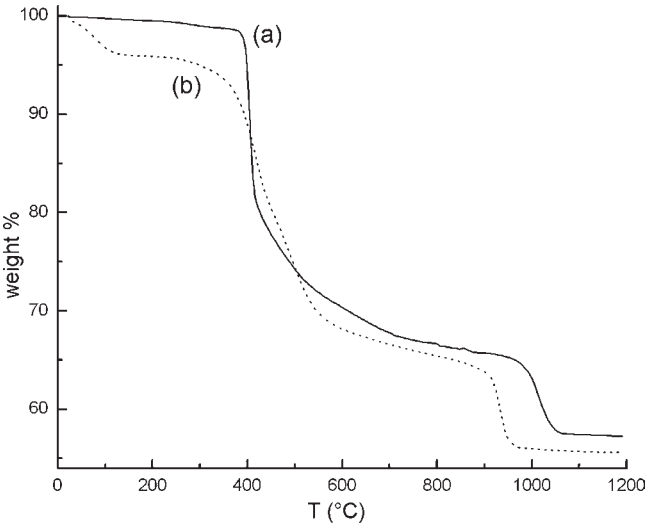

Figure 6. TGA curves for ZPD (a) and ZBPD (b).

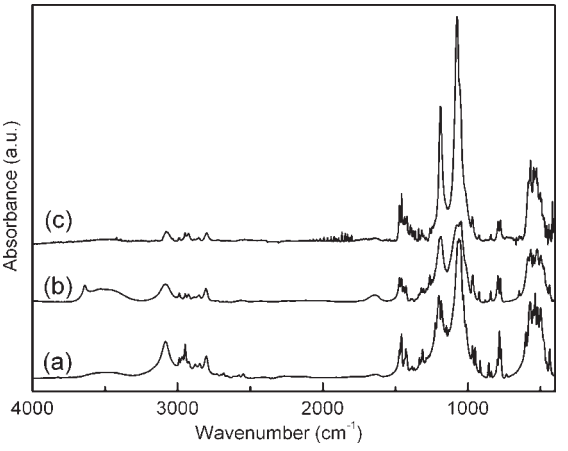

Figure 7. FT-IR absorption spectra of ZPD (a), ZBPD (b), and ZBPDa (c).

Under this hypothesis, the experimental weight losses (41.43% for ZPD and 44.50% for ZBPD) are in good agreement with those calculated (40.53 and 42.84%, respectively).

Vibrational Spectroscopy. The FT-IR and Raman spectroscopic features for ZPD and ZBPD are discussed and compared with those of zirconium fluoride aminodiphosphonate containing a butanoic group, $ZrHF(O_3PCH_2)_2NHC_3H_6CO_2$ (hereafter ZB),[2f] and zirconium difluoride aminodiphosphonate containing a piperazine group, $ZrF_2(O_3PCH_2)_2(NH)_2C_4H_8$ (hereafter ZPIP).[3]

FT-IR analysis. Figure 7 shows the FT-IR spectra of ZPD and ZBPD, while Figure 8 reports those of ZB and ZPIP for comparison.

The spectra of ZPD and ZBPD are very similar, reflecting the high of similarity of their structures.

The band at 3080 cm^{-1} can be ascribed to the H−F stretching vibration, thus confirming the presence of a protonated fluorine ligand coordinated to the metal atom. This assignment was made on the basis of a comparison with the spectrum of ZB, which also contains an analogous ligand on zirconium (see Figure 8). In ZB, the disappearance of this band after heating at 240 °C was attributed to the loss of HF. As a

dx.doi.org/10.1021/ic201381t |*Inorg. Chem.* 2011, 50, 10835–10843

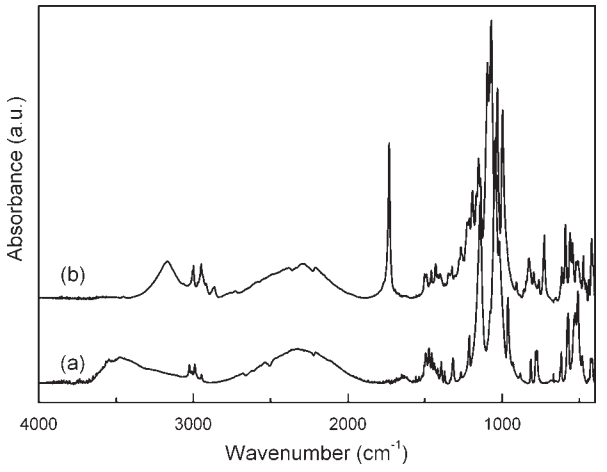

Figure 8. FT-IR spectra of ZB (a) and ZPIP (b).

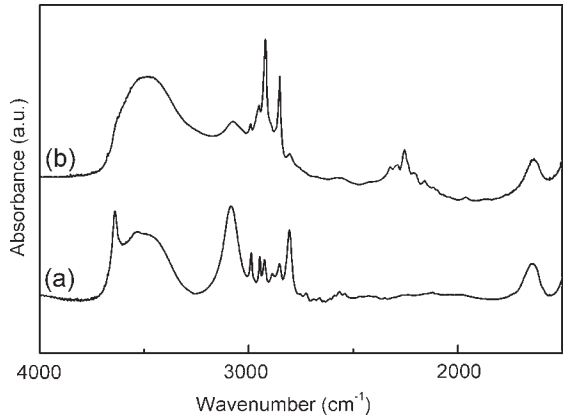

Figure 9. FT-IR spectra of ZBPD before (a) and after (b) isotopic H/D exchange.

further support to this assignment, H/D exchange was performed on ZBPD (Figure 9): the exchanged sample shows that the intensity of the H−F band is strongly reduced, while a new band that can be assigned to the D−F stretching arises at 2050 cm^{-1}, in good agreement with the expected value of 2035 cm^{-1}, calculated by taking into account the reduced mass of the D−F group.

The total absence of the broad band between 2600 and 2200 cm^{-1}, assigned to the R_3N-H^+ bond, and also present in ZB and ZPIP, indicates that the nitrogen atoms of the piperidine rings are not protonated.

The C−H stretching vibration bands are very evident near 3000 cm^{-1}.

The complex system of bands in the region 1500−400 cm^{-1} is due to vibrations of the rest of the framework. Some qualitative assignments can be done: the bands between 1500 and 1400 cm^{-1} are related to the C−H bending modes; the strong bands in the 1200−900 cm^{-1} region can be assigned to the P−O stretching modes, which overlap with the weaker C−N−C stretchings; the bands around 800 cm^{-1} are due to the C−C stretching vibrations; in the region between 600 and 400 cm^{-1}, the Zr−O stretching and P−O, P−C, C−C, and C−N bending vibrations can be found.[11]

The presence of crystallization water in ZBPD is documented by the absorption bands around 3500 and 1600 cm^{-1}. In particular, the

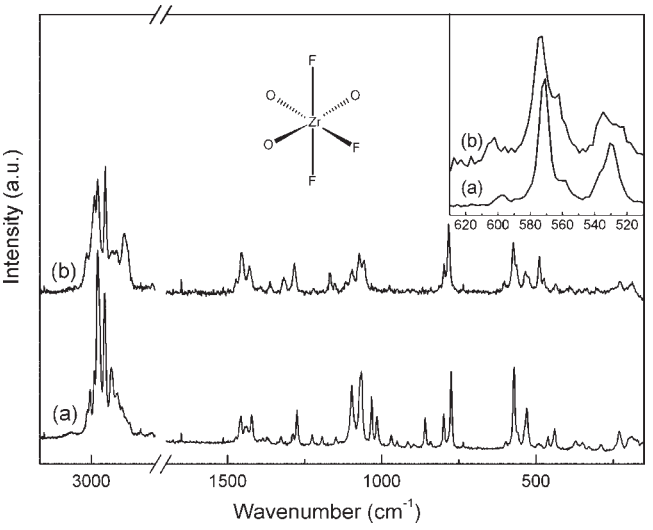

Figure 10. Raman spectra of ZPD (a) and ZBPD (b). An expansion of the region between 500 and 600 cm^{-1} is also shown.

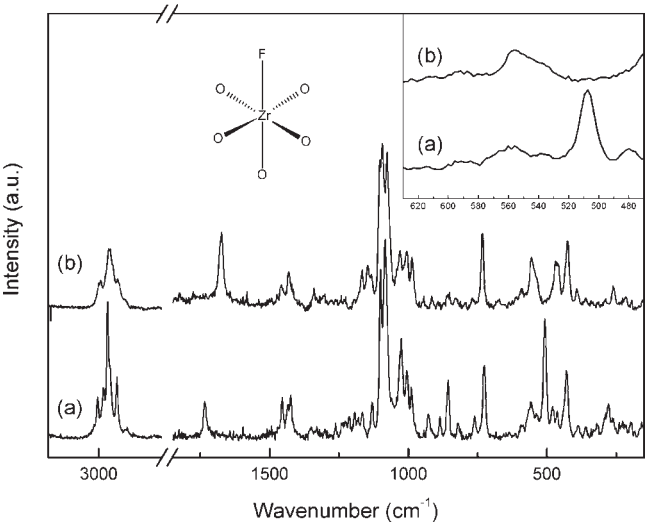

Figure 11. Raman spectra of ZB before (a) and after (b) the loss of HF. An expansion of the region between 500 and 600 cm^{-1} is also shown.

presence of a sharp band at 3640 cm^{-1}, typical of OH groups noninteracting with hydrogen bonds, superimposed to the broad band typical of bonded water, may suggest that water molecules experience different kinds of interactions inside the structure, in agreement with the structural disorder found by Rietveld refinement. These bands completely disappear on ZBPDa.

On the contrary, similar absorption bands observed in the FT-IR spectrum of ZPD must be related to surface-adsorbed humidity because the other analytical and structural information exclude the presence of crystallization water.

Raman Analysis. The Raman spectra of ZPD and ZBPD are reported in Figure 10, while those of ZB and ZPIP are reported in Figures 11 and 12, respectively.

Raman spectroscopy is mainly used here to investigate the Zr−F environment in the different structures. In this relation, the most significant signals in Raman spectra are found in the region between 500 and 600 cm^{-1}, corresponding to the metal−fluorine bond stretching frequency range, as found in the literature.[12]

dx.doi.org/10.1021/ic201381t |*Inorg. Chem.* 2011, 50, 10835–10843

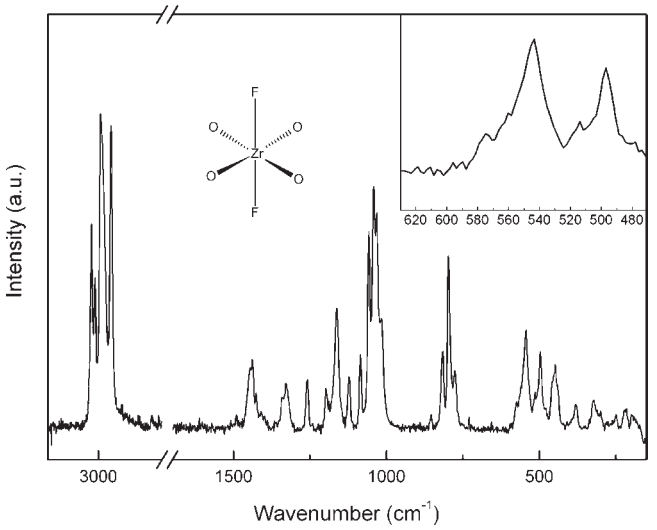

Figure 12. Raman spectrum of ZPIP. An expansion of the region between 500 and 600 cm^{-1} is also shown.

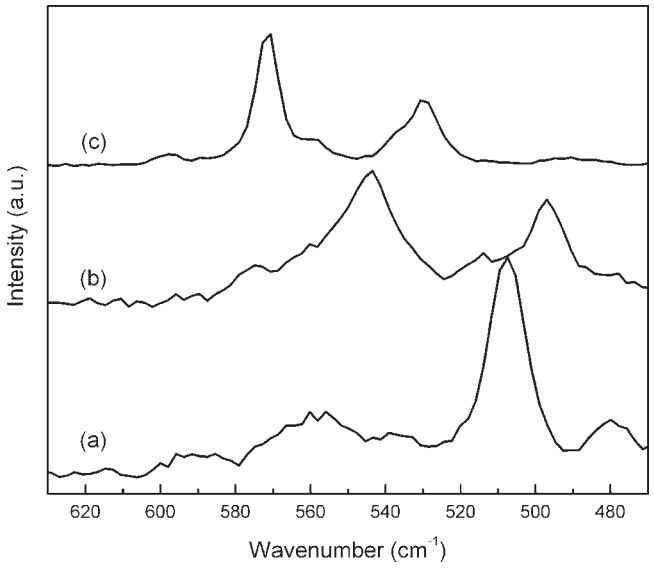

Figure 13. Comparison of the Raman spectra of ZB (a), ZPIP (b) and ZPD (c) in the region between 500 and 600 cm^{-1}.

We particularly refer to the work of Preetz and Erlhöfer,[13] who deal with octahedral fluorochloroplatinates(IV) with different degrees of substitution; these systems have the same coordination geometry and metal oxidation number (which are relevant parameters influencing the vibrational behavior of metal−halogen bonds) as our compounds and, despite the different metal atom, have been usefully used as terms of comparison for the assignment and interpretation of our spectra.

The number of fluorine atoms in the coordination sphere of zirconium increases when moving from ZB (one fluorine), through ZPIP (two fluorines), up to ZPD and ZBPD (three fluorines). These changes influence the position and, for piperidine compounds, the number of signals.

In ZB, containing ZrO_5F octahedra, the band at 507 cm^{-1} corresponds to the Zr−F stretching, and clear evidence supporting this assignment is its disappearance after heating of the compound at 240 °C, when HF is lost (Figure 10).[2f] For comparison, the corresponding Pt−F vibration band of the analogous $PtCl_5F$ system is found at 509.1 cm^{-1}.[13b]

In ZPIP, containing ZrO_4F_2 octahedra with fluorine atoms in the trans position, the signal at 544 cm^{-1} has been assigned to the *trans*-F−Zr−F symmetric stretching (Figure 11). The corresponding band of the $PtCl_4F_2$ system is at 549.5 cm^{-1}, with a similar shift of about 40 cm^{-1} toward higher frequencies, with respect to the previous compounds.

In ZPD and ZBPD, having ZrO_3F_3 octahedra in *mer* (or trans) configuration, there are two different signals: one is at 530 cm^{-1}, which is due to the stretching of the bond between zirconium and the central fluorine, and a second stronger band at 570 cm^{-1}, which can be ascribed to the *trans*-F−Zr−F symmetric stretching (Figure 9). In $PtCl_3F_3$ systems, these bands lie at 500.6 and 554.7 cm^{-1}, respectively.

Figure 13 resumes the Raman spectra of ZB, ZPIP, and ZPD, in the region between 500 and 600 cm^{-1}.

Discussion. The analogies revealed between the structures of ZPD and ZBPDa reflect the structural analogies of constituting phosphonate building blocks PD and BPD: BPD can be considered as originating from the connection of two units of PD via a C−C bond; in the same way, the layered structure of ZBPD can be seen as originating from the lateral connection of adjacent chains of ZPD. Therefore, these structures show the same relationships as the molecular structure of their building blocks. However, at the moment, these analogies can hardly be used for a reliable structural prediction because these systems possess a somewhat embarrassing variability. For example, as was already cited in the Introduction, the clear relationships between the molecular structures of BPD and *N*,*N*′-bis(phosphonomethyl)piperazine[3] are not transferred to the structures of their zirconium derivatives as an isoreticular relationship. It is worth noting that all of our attempts to perform syntheses by changing various parameters (pH, concentration of reagents, solvent, temperature, etc.) only produced ZPD and ZBPD.

In previous studies, we pointed out that the presence of a fluorine atom in the zirconium coordination sphere was associated with the presence of a PO···N noncovalent strong interaction, which diverts a P−O group from zirconium and leaves one coordination site to fluorine. In particular, for piperazine derivatives, we observed that the presence of such PO···N interactions depended on the pH of the synthesis mixture. On the contrary, in the present compounds, zirconium is bonded to three fluorine atoms, although no P−O groups are involved in noncovalent interactions. Accordingly, the pH of the synthesis was found not to be a sensible parameter. At the moment, we cannot explain this behavior.

The same relationship existing between the molecular structures of PD and BPD is also present in two phosphonic acids derived from pyridine and 4,4′-bipyridine (Figure 14), although these latter compounds are aromatic and there is an ethylene spacer in place of a methylene between nitrogen and phosphorus. Notwithstanding, their zirconium derivatives (hereafter identified as ZPY and ZBPY; Figure 14)[2b,j] did not show similar structural analogies found in the ZPD−ZBPD couple. Indeed, the structure of ZBPY is very similar to that of ZBPD: the same type of layers, the same connectivity of building blocks, and the same fluorine atom contents. In contrast, the ZPY structure is sensibly different from ZPD, despite their similar composition, because it shows a *fac* (or cis) configuration of the three fluorine atoms bonded to zirconium, and it features all-inorganic layers

dx.doi.org/10.1021/ic201381t |*Inorg. Chem.* 2011, 50, 10835–10843

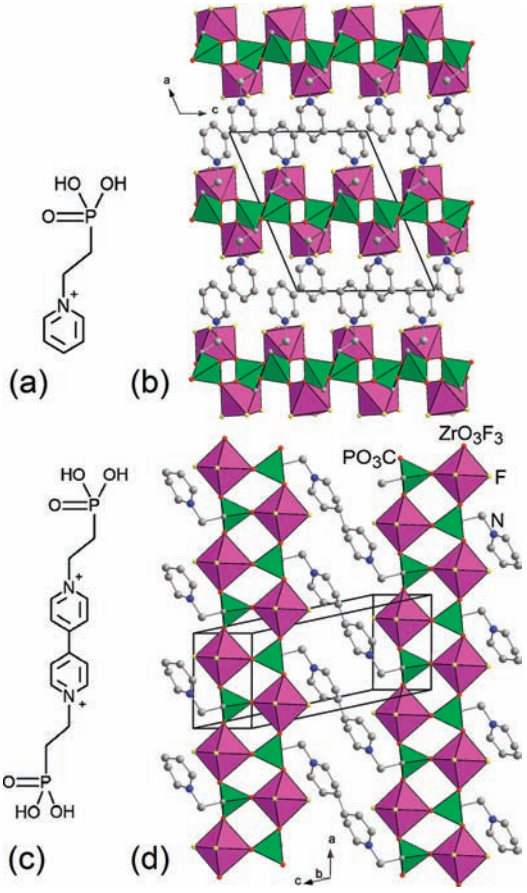

Figure 14. Views of the structure of *N*-(phosphonoethyl)pyridinium (a), its zirconium derivative ZPY, (b), *N*,*N*′-bis(phosphonoethyl)-4,4′-bipyridinium (c), and its zirconium derivative ZBPY (d). Hydrogen atoms are omitted.

made of the connectivity of only zirconium octahedra and phosphorus tetrahedra. The pyridine groups are pending on the surface of the layers and point toward the interlayer regions. A partial explanation of these differences can be found in the different abilities of these two systems to form $\pi-\pi$-stacking interactions. For ZPY, the aromatic rings pending from adjacent layers are able to interact via $\pi-\pi$ stacking in groups of two, introducing a structure-directing factor, able to induce a different spatial arrangement, while in ZPD, the piperidine rings cannot behave likewise.

In conclusion, the same relationships between PD and BPD building blocks, which can justify the structural analogies present in their zirconium derivatives, cannot be applied for ethylpyridinium and ethylbipyridinium systems. Reasons explaining their similarities or differences sometimes can be found (the presence of noncovalent interactions, electroneutrality, etc.) and sometimes not. In addition, even when clearly present, these relationships often involve a limited number of compounds. Nevertheless, these short correlations represent a small nucleus of knowledge to be taken into account and combined with future observations for a deeper understanding of the stereochemistry of zirconium phosphonate systems.

CONCLUSIONS

In summary, two new zirconium phosphonates were synthesized by the HF method. Fluoride ions, besides acting as masking agents for zirconium, by reducing the saturation degree of precipitating solutions and allowing good crystallization of precipitates, were found to participate in building of the solids and deeply affect the resulting crystal structures, which were determined ab initio by PXRD data. In addition, a thorough spectroscopic investigation involving FT-IR and Raman techniques confirmed and completed the description of some structural details that cannot be easily studied by conventional powder diffraction analysis, including investigation of the F···N hydrogen bond, by means of H/D isotopic exchange, which allowed the unambiguous assignment of the hydrogen atom to the fluorine ligand.

A comparative discussion on the relationships between the structures of various phosphonate building blocks and those of their zirconium derivatives was done in search of useful evidence for a reliable structural prediction for this class of compounds. Although at the moment this goal seems far from being reached, the structural versatility shown by zirconium phosphonates can offer new opportunities in inorganic chemistry even after 30 years of research on this topic.

ASSOCIATED CONTENT

Supporting Information. Crystallographic information files in CIF format for ZPD and ZBPDa, tables with complete crystallographic parameters for ZPD and ZBPDa, and a comparison between PXRD patterns of ZBPD and ZBPDa. This material is available free of charge via the Internet at http://pubs.acs.org.

AUTHOR INFORMATION

Corresponding Author
*E-mail: marcotaddei@hotmail.com.

ACKNOWLEDGMENT

This work was supported by the Italian Ministry of University and Research under Project PRIN 2007. The authors thank Gloria Di Domenicantonio Scarcamazza for her contribution to the synthetic work and Paola Sassi and Alessandra Giugliarelli for their contributions to FT-IR measurements.

REFERENCES

(1) (a) Alberti, G. In *Comprehensive Supramolecular Chemistry*; Alberti, G., Bein, T., Eds.; Pergamon Press: Oxford, U.K., 1996; Vol. 7, Chapter 5. (b) Clearfield, A. Costantino, U. In *Comprehensive Supramolecular Chemistry*; Alberti, G., Bein, T., Eds.; Pergamon Press: Oxford, U.K., 1996; Vol. 7, Chapter 4. (c) Clearfield, A. In *Progress in Inorganic Chemistry*; Karlin, K. D., Ed.; John Wiley & Sons: New York, 1998; Vol. 47, pp 374−510. (d) Alberti, G.; Casciola, M.; Costantino, U.; Vivani, R. *Adv. Mater.* **1996**, *8*, 291. (e) Alberti, G.; Casciola, M. *Solid State Ionics* **2001**, *145*, 3–16. (f) Casciola, M.; Capitani, D.; Comite, A.; Donnadio, A.; Frittella, V.; Pica, M.; Sganappa, M.; Varzi, A. *Fuel Cells* **2008**, *3*, 217–224.

(2) (a) Vivani, R.; Alberti, G.; Costantino, F.; Nocchetti, M. *Microporous Mesoporous Mater.* **2008**, *107*, 58. (b) Vermeulen, L. A.; Fateen, R. Z.; Robinson, P. D. *Inorg. Chem.* **2002**, *41*, 2310–2312. (c) Vivani, R.; Masci, S.; Alberti, G. *Inorg. Chem.* **2004**, *43*, 368. (d) Poojary, D. M.; Zhang, B.; Clearfield, A. *Angew. Chem., Int. Ed. Engl.* **1994**, *33*, 2324. (e) Costantino, U.; Nocchetti, M.; Vivani, R. *J. Am. Chem. Soc.* **2002**, *124*, 8428–8434. (f) Vivani, R.; Costantino, U.; Nocchetti, M. *J. Mater. Chem.* **2002**, *12*, 3254–3260. (g) Vivani, R.; Costantino, U.; Nocchetti, M.; Costantino, F. *Inorg. Chem.* **2006**, *45*, 2388–2390. (h) Vivani, R.; Costantino, F.; Nocchetti, M.; Gatta, G. D. *J. Solid State Chem.* **2004**,

177, 4013–4022. (i) Zhang, B.; Poojary, D. M.; Clearfield, A. *Inorg. Chem.* **1998**, *37*, 249. (j) Poojary, D. M.; Vermeulen, L. A.; Vicenzi, E.; Clearfield, A.; Thompson, M. E. *Chem. Mater.* **1994**, *6*, 1845.

(3) Taddei, M.; Costantino, F.; Vivani, R. *Inorg. Chem.* **2010**, *49*, 9664–9670.

(4) (a) Wharmby, M. T.; Mowat, J. P. S.; Thompson, S. P.; Wright, P. A. *J. Am. Chem. Soc.* **2011**, *133*, 1266–1269. (b) Eddaoudi, M.; Kim, J.; Rosi, N.; Vodak, D.; Wachter, J.; O'Keeffe, M.; Yaghi, O. M. *Science* **2002**, *295*, 469–472. (c) Park, Y. K.; Choi, S. B.; Kim, H.; Kim, K.; Won, B.-H.; Choi, K.; Choi, J. S.; Ahn, W.-S.; Won, N.; Kim, S.; Jung, D. H.; Choi, S. H.; Kim, G. H.; Cha, S.-S.; Jhon, Y, H.; Yang, J. K.; Kim, J. *Angew. Chem., Int. Ed.* **2007**, *46*, 8230–8233.

(5) Moedritzer, K.; Irani, R. R. *J. Org. Chem.* **1966**, *31*, 1603.

(6) Werner, P. E.; Eriksson, L.; Westdhal, M. *J. Appl. Crystallogr.* **1985**, *18*, 367.

(7) Boultif, A.; Louer, D. *J. Appl. Crystallogr.* **2004**, *37*, 724.

(8) Favre-Nicolin, V.; Cerny, R. *J. Appl. Crystallogr.* **2002**, *35*, 734.

(9) Falcioni, M.; Deem, M. W. *J. Chem. Phys.* **1999**, *110*, 1754.

(10) Larson, C.; von Dreele, R. B. *Generalized Crystal Structure Analysis System*; Los Alamos National Laboratory: Los Alamos, NM, 2001.

(11) Socrates, G. *Infrared and Raman Characteristic Group Frequencies: Tables and Charts*; John Wiley & Sons: Chichester, U.K., 2001.

(12) (a) Clark, R. J. H.; Errington, W. *J. Chem. Soc.* **1967**, 258–261. (b) Toth, L. M.; Quist, A. S.; Boyd, G. E. *J. Phys. Chem.* **1973**, *77*, 1384–1388. (c) Kawamoto, Y.; Sakaguchi, F. *Bull. Chem. Soc. Jpn.* **1983**, *53*, 2138–2141. (d) Kruger, A.; Heyns, A. M. *Vib. Spectrosc.* **1997**, *14*, 171–181. (e) Dracopoulos, V.; Vagelatos, J.; Papatheodorou, G. N. *J. Chem. Soc., Dalton Trans.* **2001**, 1117–1122. (f) Davidovich, R. L.; Logvinova, V. B.; Kaidalova, T. A.; Gerasimenko, A. V. *Russ. J. Inorg. Chem.* **2007**, *52*, 742–748.(g) Nakamoto, K. *Infrared and Raman Spectra of Inorganic and Coordination Compounds*; John Wiley & Sons: Hoboken, NJ, 2009.

(13) (a) Preetz, W.; Erlhöfer, P. *Z. Natuforsch.* **1989**, *44b*, 412–418. (b) Erlhöfer, P.; Preetz, W. *Z. Natuforsch.* **1989**, *44b*, 1214–1220.